JOURNAL OF COMPUTATIONAL PHYSICS 46, 429–453 (1982)

Kernel Estimates as a Basis for General Particle Methods in Hydrodynamics

R. A. GINGOLD* AND J. J. MONAGHAN

Department of Mathematics, Monash University, Clayton, Victoria 3168, Australia

Received April 10, 1979; revised March 17, 1981

The general theory of kernel estimation is discussed and applied to particle methods in hydrodynamics. We show that a simple form of estimation leads to a particle method which does not require a grid and satisfies the conservation laws very accurately. The merits of different kernels are examined, and numerical tests of their ability to reproduce known densities are described. Examples of the application of the new particle method to isothermal shocks, to the collapse of gas clouds, and to the tidal interaction of stars are described.

1. INTRODUCTION

In the Lagrangian description of a fluid the concept of a fluid element is fundamental, and the motion of the fluid can be represented with arbitrary accuracy by the motion of a sufficiently large number of such elements. For theoretical work the fluid elements are considered infinitesimal. The resulting equations are not often used because they are cumbersome unless the fluid possesses a simple geometrical symmetry. The finite-difference version of the equations can be used in numerical work, but frequent reorganization of the mesh is required if there is severe shear. In spite of these difficulties the Lagrangian description is attractive because it does have advantages over the Eulerian description for certain problems. For example, in the tidal disruption of a star, thin filaments are formed, and the construction of a suitable Eulerian mesh for these moving filaments is complicated. The Lagrangian description puts the mesh where the material is and it should, in principle, lead to a more economical calculation. It has the further advantage that it is free from errors arising from the convective $(\mathbf{v} \cdot \nabla)$ term.

The principal difficulties of the Lagrangian description can be removed if the fluid elements are considered to be small, but not infinitesimal. The continuous fluid is then approximated by particles or fluid elements. An interpretation of a one-dimensional finite-difference Lagrangian scheme, as a particle model with interpar-

* Present address: Mt. Stromlo and Siding Spring Observatories, Australian National University, Private Bag WODEN P. O., Woden, ACT 2606, Australia.

0021-9991/82/060429-25$02.00/0

ticle forces derived from the pressure, was given by Von Neumann [1]. Pasta and Ulam [2] also discussed a finite particle scheme with forces chosen to simulate the pressure, and a variant of their method has recently been proposed by Larson [3]. The commonly used particle methods (PIC, GAP, CIC, and the method due to Leboef *et al.* [4] referred to hereafter as LTD) use a grid to facilitate the computation of the forces on the particles. Although the latter methods differ in detail, they have the common feature that the properties of the particles (mass, velocity etc.) are interpolated to the grid. The forces are found by finite differences on the grid after which they are interpolated back to particles. The process incorporates a series of smoothing operations with the grid providing the natural length scale.

The particle method we describe here differs from those discussed above in the way the fluid parameters are determined from the particle positions and properties. As ordinarily defined, the density ρ for particles of equal mass, is proportional to the number of particles per unit volume. It may, however, be considered from a statistical point of view: the probability that a particle is found in the volume element ΔV is proportional to $\rho \Delta V$. If the statistical point of view is carried over to the system of fluid elements, the density can be defined in the same way. We regard the positions of the fluid elements as a random sample from a probability density proportional to the mass density. The estimation of the density is then equivalent to estimating a probability density from a sample. Known statistical methods based on smoothing kernels (Rosenblatt [5, 6]; Boneva *et al.* [7]) can be used for this purpose.

The statistical estimation of density by smoothing kernels can be interpreted as the replacement of each particle by a smoothed-out density (hence we call it smoothed particle hydrodynamics SPH). A similar interpretation can be given (see Section 2) of the procedure used for density estimation in PIC, GAP, CIC, and LTD. Our method departs from these by eliminating the grid both in the density estimation, and in the estimation of the forces on the particles. The resulting numerical method is very simple to program, is robust in operation, and conserves energy and momentum accurately. Furthermore, because the grid has been eliminated, the resolution is determined by the particle separation and a significant improvement in resolution can be achieved (see Section 5a).

The plan of this paper is to describe the theory of kernel estimation in Section 2 and show how the pressure forces can be calculated without the use of a mesh. In Section 3 we examine various smoothing kernels, and in Section 4 we discuss the choice of smoothing length. Applications are given in Section 5. The computational details are given in the Appendix.

2. Kernel Estimation

We consider first the calculation of the density. If we have a set of particles of equal mass, the density can be considered either as proportional to the average number of particles per unit volume, or as proportional to probability density of

finding a particle in a given volume element. With the latter interpretation we consider the estimate of the true density ρ,

$$\rho_s(\mathbf{r}) = \int W(\mathbf{r} - \mathbf{r}', h)\, \rho(\mathbf{r}')\, d\mathbf{r}', \tag{2.1}$$

where

$$\int W(\mathbf{r}, h)\, d\mathbf{r} = 1, \tag{2.2}$$

and the integration is over all space. The parameter h defines the smoothing length of the kernel W. In general, W may depend on several parameters. Because of (2.2) the total mass M is independent of the estimation since

$$M = \int \rho_s(\mathbf{r}, h)\, d\mathbf{r} = \int \rho(\mathbf{r})\, d\mathbf{r}. \tag{2.3}$$

If W is a δ function, then $\rho_s(\mathbf{r}) = \rho(\mathbf{r})$. In practice W is chosen to be a member of a sequence of functions which approximates a δ function. In one dimension, if $F(x)$ is integrable in $-\infty < x < \infty$, then W can be defined by

$$W(x) = \frac{1}{h} F\left(\frac{x}{h}\right) \Big/ \int_{-\infty}^{\infty} F(u)\, du. \tag{2.4}$$

Other conditions on W will be discussed below.

Since $\rho(\mathbf{r}')$ is unknown, (2.1) cannot be evaluated directly, but if we have a set of N points (in the hydrodynamical problem they will be the positions of the particles) $\mathbf{r}_1, \mathbf{r}_2, \ldots, \mathbf{r}_N$ randomly distributed according to ρ, the integral can be evaluated by the Monte Carlo method. Thus, defining $\rho_{sN}(\mathbf{r})$ by

$$\rho_{sN}(\mathbf{r}) = \frac{M}{N} \sum_{j=1}^{N} W(\mathbf{r} - \mathbf{r}_j, h), \tag{2.5}$$

we find, with E denoting the expectation, that if h is independent of the sample, then

$$E[\rho_{sN}(\mathbf{r})] = \rho_s(\mathbf{r}). \tag{2.6}$$

Since W can be chosen to be arbitrarily differentiable, the derivatives of ρ can be calculated easily from (2.5) without using finite differences.

In problems involving large changes in density (the collapse of a protostar is an example) h must be related to the set of points. In this case (2.6) is approximately true with h replaced by its expected value.

To ensure that $\rho_s(\mathbf{r}) \to \rho(\mathbf{r})$ as $N \to \infty$ we require only that $h \to 0$ as $N \to \infty$. In statistical practice the dependence of h on N is limited by the need to keep fluc-

tuations from growing too rapidly. In hydrodynamic problems the fluctuations are normally low, and it is appropriate to take

$$h \propto 1/N^{1/d}, \tag{2.7}$$

where d is the number of dimensions. Further consideration of h will be deferred to Section 4.

In the usual particle methods PIC, GAP, CIC, and LTD, estimates of the density and the thermal energy per unit volume at mesh points are special cases of kernel estimates. We illustrate the relationship of these methods to kernel smoothing for a typical case in which we assume the particle is smoothed in space according to the function $G(\mathbf{u})$, then area weighted to the nearest mesh points. The density ρ_λ at the mesh point $\mathbf{r}_\lambda$ is then

$$\rho_\lambda = \frac{M}{N} \sum_{j=1}^{N} \int R(\mathbf{r} - \mathbf{r}_\lambda)\, G(\mathbf{r} - \mathbf{r}_j)\, d\mathbf{r}, \tag{2.8}$$

where the function $R(\mathbf{r}) \equiv R(x)\, R(y)\, R(z)$ with

$$\begin{aligned} R(u) &= \frac{1}{\Delta}\left(1 - \frac{|u|}{\Delta}\right); && |u| \leqslant \Delta \\ &= 0; && |u| > \Delta \end{aligned} \tag{2.9}$$

produces area weighting on a mesh with interval Δ.

Estimate (2.8) is a kernel estimate with kernel

$$W(\mathbf{r}_\lambda - \mathbf{r}_j) = \int R(\mathbf{u})\, G(\mathbf{u} - (\mathbf{r}_j - \mathbf{r}_\lambda))\, d\mathbf{u}. \tag{2.10}$$

If G is a Gaussian, then (2.8) is the CIC algorithm for ρ_λ. If G is a δ function, then (2.8) is the GAP algorithm. The CIC algorithm results in a density which is smoother than that calculated by GAP, but it is neither smoother nor more accurate than the density obtained using (2.5) with a Gaussian kernel. As we show in Section 3, the smoothness and accuracy of estimates made with kernels having similar analytical properties depends primarily on the smoothing length. Since the Gaussian kernel and (2.10) with G a Gaussian have similar analytical properties, we expect both kernels to give very similar estimates.

In the same way the thermal energy per unit volume $\varepsilon\rho$ can be estimated by using the integral

$$\int \rho(\mathbf{r}')\, \varepsilon(\mathbf{r}')\, W(\mathbf{r} - \mathbf{r}')\, d\mathbf{r}', \tag{2.11}$$

which leads to the estimate

$$\frac{M}{N} \sum_{j=1}^{N} \varepsilon_j\, W(\mathbf{r} - \mathbf{r}_j). \tag{2.12}$$

By choosing W appropriately in (2.12) the algorithms used in the particle methods PIC, CIC, GAP, and LTD can be recovered.

The mesh was introduced in particle codes both to allow estimates to be made of fluid variables and to allow forces to be calculated by finite differences. The forces on the particles could then be calculated by interpolation from the mesh. In many cases this procedure is equivalent to a kernel estimate but, as we show below, the kernel is unnecessarily complicated for the accuracy it achieves.

We consider a one-dimensional problem, and assume the pressure gradient is to be calculated from the density and thermal energy gradients. The density and thermal energy are known at the mesh points from kernel estimates. To calculate the derivative $\partial\rho/\partial x$ at the point x_i (the position of particle i) we first use finite differences to calculate $\partial\rho/\partial x$ at the mesh point x_λ. An appropriate form is

$$\frac{\rho_{\lambda+1}-\rho_\lambda}{\Delta}=\frac{M}{N}\sum_{j=1}^{N}\frac{\partial}{\partial x_\lambda}\int R(x-x_\lambda)\,G(x-x_j)\,dx \tag{2.13}$$

where (2.8) and (2.9) have been used. Interpolation using area weighting gives the approximation for the derivative at x_i,

$$\sum_\lambda\left(\frac{\rho_{\lambda+1}-\rho_\lambda}{\Delta}\right)R(x_i-x_\lambda). \tag{2.14}$$

The relation between (2.14) and a kernel estimate of a density can best be seen by replacing $\sum_\lambda$ by an integral. Substituting (2.13) into the resulting integral, and integrating by parts, we find that (2.14) becomes

$$\frac{\partial}{\partial x_i}\frac{M}{N}\sum_{j=1}^{N}W(x_i-x_j), \tag{2.15}$$

where

$$W(x_i-x_j)=\iint R(x_i-s)\,R(x-s)\,G(x-x_j)\,dx\,ds. \tag{2.16}$$

In the approximation implied by $\sum_\lambda\to\int$ (which is consistent with the finite-difference estimate (2.13)) the entire procedure is equivalent to making a kernel estimate of the density and differentiating it analytically. Since the kernel (2.16) has no advantages over a Gaussian kernel, the entire finite-difference procedure is superfluous. The mesh can be bypassed and (2.5) used directly with a Gaussian kernel. The same conclusion holds for the thermal energy gradient. In PIC, CIC, GAP, and the finite-difference version of LTD (required for nonperiodic conditions) the force calculation is not usually an exact kernel estimate, but it is a close approximation to a kernel estimate with a kernel which has all the disadvantages of the kernel (2.16). Accuracy equivalent to that achieved in these methods can be achieved by using kernel estimates such as (2.5) directly with a suitable kernel (see Section 3). In practice, with a given number of particles, removing the mesh has the further advantage that

the accuracy is improved because the smoothing length of the kernel is only limited by the particle separation. As we show in Section 5 a significant improvement in resolution over the mesh based method LTD can be achieved. In the remainder of this paper we refer to kernel-based methods which do not use a mesh as smoothed particle hydrodynamics (SPH).

The pressure gradient in SPH can be calculated from a kernel estimate of the pressure P. We use the smoothed pressure P_s defined by

$$\begin{aligned} P_s(\mathbf{r}) &= \int W(\mathbf{r}-\mathbf{r}', h)\, P(\mathbf{r}')\, d\mathbf{r}', \\ &= \int W(\mathbf{r}-\mathbf{r}', h)(P/\rho)\, \rho(\mathbf{r}')\, d\mathbf{r}'. \end{aligned} \tag{2.17}$$

The estimate of P is then

$$P_{sN}(\mathbf{r}) = \frac{M}{N} \sum_{j=1}^{N} \frac{P_j}{\rho_j} W(\mathbf{r}-\mathbf{r}'). \tag{2.18}$$

The pressure force per unit mass on a particle at $\mathbf{r}$ is then

$$-\frac{1}{\rho}\nabla P_{sN} = -\frac{M}{N}\frac{1}{\rho} \sum_{j=1}^{N} \frac{P_j}{\rho_j} \nabla W(\mathbf{r}-\mathbf{r}'). \tag{2.19}$$

A variety of further expressions for $\nabla P/\rho$ are possible depending on the way $\nabla P/\rho$ is written. We consider two. Writing

$$-\frac{1}{\rho}\nabla P = -2\frac{\sqrt{P}}{\rho}\nabla\sqrt{P}, \tag{2.20}$$

we estimate $\sqrt{P}$ in the same way as P in (2.17). Then

$$-\frac{1}{\rho}\nabla P \to -2\frac{\sqrt{P}}{\rho}\sum_j \frac{\sqrt{P_j}}{\rho_j}\nabla W(\mathbf{r}-\mathbf{r}'). \tag{2.21}$$

If we write

$$-\frac{1}{\rho}\nabla P = -\nabla\left(\frac{P}{\rho}\right) - \frac{P}{\rho^2}\nabla\rho \tag{2.22}$$

and use a kernel estimate of P/ρ and ρ, we find

$$-\frac{1}{\rho}\nabla P \to -\frac{M}{N}\sum_{j=1}^{N}\frac{P_j}{\rho_j^2}\nabla W(\mathbf{r}-\mathbf{r}_j) - \frac{M}{N}\frac{P}{\rho^2}\sum_{j=1}^{N}\nabla W(\mathbf{r}-\mathbf{r}_j). \tag{2.23}$$

The three expressions for the pressure force ((2.19), (2.21), and (2.23)) have a similar accuracy and the correct limit as $h \to 0$ and $N \to \infty$, but they conserve momentum and energy differently. Expression (2.19) conserves neither energy nor momentum in

general. Momentum is conserved exactly if (2.21) and (2.23) are used and W is an even function. If h is constant (2.23) conserves both energy and momentum when $P = P(\rho)$. If h depends on the particle positions, very accurate energy conservation and exact momentum conservation can be achieved by deriving the equations of motion from a Lagrangian. For a nondissipative, isentropic gas with no body forces, the exact Lagrangian (Eckart [8]) is

$$\int [\tfrac{1}{2}\dot{\mathbf{r}}^2 - U(\rho)]\,\rho\,dr, \tag{2.24}$$

where U is the internal energy. Evaluating (2.24) by the Monte Carlo method we arrive at the Lagrangian

$$L = \frac{M}{N}\sum_{j=1}^{N} (\tfrac{1}{2}\dot{\mathbf{r}}_j^2 - U(\rho_j)). \tag{2.25}$$

Denoting $dU/d\rho$ by U' the equation of motion of the kth particle is

$$\ddot{\mathbf{r}}_k = -\sum_{j=1}^{N} [U'(\rho_j) + U'(\rho_k)] \left\{\frac{\partial}{\partial \mathbf{r}_k} W(\mathbf{r}_k - \mathbf{r}_j, h)\right\}_{h\,\text{const}} + \left\{\frac{\partial}{\partial h}\sum_j - U(\rho_j)\right\} \frac{\partial h}{\partial \mathbf{r}_k}, \tag{2.26}$$

where the right-hand side of (2.26) is $\partial L/\partial \mathbf{r}_k$.

Recalling that $U' = P/\rho^2$ the first summation in (2.26) reduces to the expression for the pressure force (2.23). It can be shown that term involving $\partial h/\partial \mathbf{r}_k$ varies with N according to $1/N^{2/d}$, where d is the number of dimensions. We therefore expect this term to become negligible for very large N.

If the system is subjected to body forces, they must be added to (2.26). The astrophysically important case of self-gravitation is described in detail in the Appendix, where details of the computational algorithm are also given.

When the evolution of the system depends on other partial differential equations (energy transport, magnetic field generation, etc.) they can be solved by using kernel estimation to evaluate spatial derivatives. In this paper, however, we confine attention to fluids with isentropic or isothermal equations of state, and body forces which are due to gravity.

3. Choosing the Smoothing Kernel

In SPH there is no grid and the density gradient is determined by differentiating ρ with respect to the particle coordinates. The smoothing kernel must therefore be differentiable at least once, and the derivative should be continuous to prevent large fluctuations in the force felt by a particle.

A further restriction on the form of the kernel comes from considering the bias β—the difference between the smoothed and true density. If, for example, $\rho(x) = \exp(-x^2/a^2)$ and the smoothing kernel is $\sqrt{\pi/h^2}\exp(-u^2/h^2)$, then

$$\rho_s(x) = \left(\frac{a^2}{a^2+h^2}\right)^{1/2} \exp\left(-\frac{x^2}{a^2+h^2}\right). \tag{3.1}$$

and the kernel alters the magnitude and spread of the density. If W has a sharp peak at $\mathbf{r} = \mathbf{r}'$ then we find, by expanding the integrand of (2.1) about $\mathbf{r}' = \mathbf{r}$, that

$$\beta = \rho_s(\mathbf{r}) - \rho(\mathbf{r}) = \nabla\rho \cdot \int \mathbf{u}\, W(\mathbf{u})\, d\mathbf{u} + \tfrac{1}{2}\int [(\mathbf{u}\cdot\nabla)(\mathbf{u}\cdot\nabla\rho)]\, \mathbf{W}\, d\mathbf{u} + \cdots. \tag{3.2}$$

The first term in the bias vanishes if $W(\mathbf{u})$ is an even function. With this choice the leading term in the bias is

$$\tfrac{1}{6}\nabla^2\rho \int u^2 W(\mathbf{u})\, d\mathbf{u} \propto h^2\, \nabla^2\rho, \tag{3.3}$$

and

$$\frac{\partial\rho_s(r)}{\partial h} \propto h. \tag{3.4}$$

The error term (3.3) can be removed by an appropriate choice of W. For example, in three dimensions, the kernel

$$\left(\frac{f}{\pi}\right)^{3/2}\left(1 - \frac{1}{4f}\nabla^2\right)e^{-fu^2}, \qquad f = \frac{1}{h^2} \tag{3.5}$$

has bias terms proportional to h^4. Such bias reducing kernels are only worth using if there are enough particles to ensure the error in the Monte Carlo integration is smaller than the bias term being eliminated.

To compare the accuracy of kernel estimates, we have examined their ability to reproduce known densities. This can be done directly by generating random numbers from a density and then attempting to recover the density by a kernel estimate. In hydrodynamic problems, however, it is usual to order the particles to ensure that large fluctuations are not built into the initial state. To simulate this situation we proceed in the following way. If D is the true density we determine D_s by integration. The particles are then allowed to move according to the equations of motion

$$\frac{d^2\mathbf{r}_i}{dt^2} = -\left[\frac{\nabla\rho}{\rho^n}\right]_i - \frac{1}{D_s^n}\nabla D_s - \gamma\frac{d\mathbf{r}_i}{dt}. \tag{3.6}$$

The term $[\nabla\rho/\rho^n]$ is calculated using the smoothed density. We have used two expressions for this term. One is based on (2.18) with $P = \rho$, and one is based on

(2.23) with $P = \rho$. The damping constant γ ensures that the particles relax to a steady state with $\rho_{sN}(\mathbf{r}_j) \doteqdot D_s(\mathbf{r}_j)$. If we had used D rather than D_s in (3.6) the particles would have settled to a configuration with ρ_{sN} very close to D. But this is inconsistent, since it implies that the particles are a sample from a density which, *when smoothed*, produces D. The constant n is chosen so that the final state is stable. If D_s is a Gaussian we choose $n = 1$; if $D_s \propto 1/(r^2 + a^2)$ we choose $n = 2$. The error in ρ_{sN} was measured by computing a mean error

$$\frac{1}{m} \sum_{i=1}^{m} |\rho_{sN}(\xi_i) - D(\xi_i)|, \tag{3.7}$$

where $\xi_i = a + (b - a)(i - 1)/(m - 1)$ and a and b are constants that depend on D_s.

In Fig. 1 we show the density estimates when D is the Gambel density $\exp(-x - \exp(-x))$ with $-\infty < x < \infty$. The density estimates were made using the two kernels

$$G(u) = (1/\pi h^2)^{1/2} \exp(-u^2/h^2), \tag{3.8}$$

and

$$\begin{aligned} P(u) &= (15/16h)(1 - u^2/h^2)^2, \qquad |u| \leqslant h \\ &= 0, \qquad\qquad\qquad\quad |u| \geqslant h, \end{aligned} \tag{3.9}$$

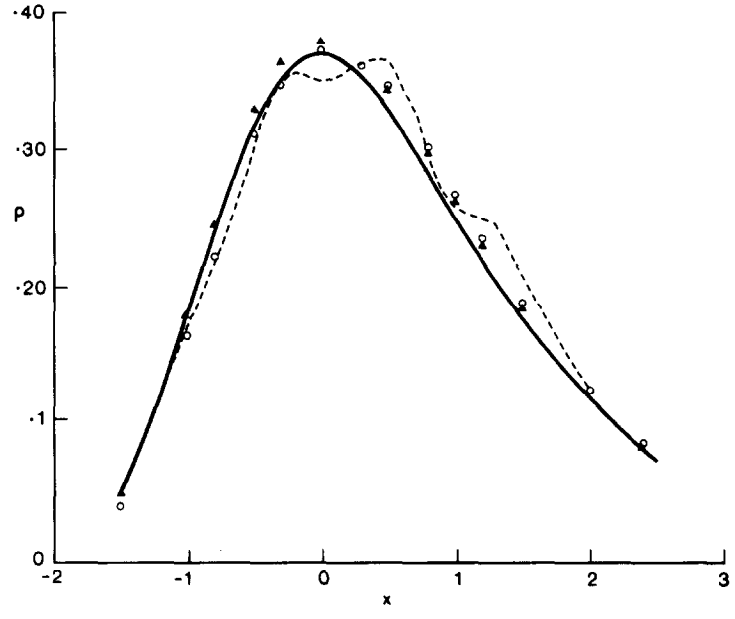

FIG. 1. Density estimates of the density $\exp(-x - e^{-x})$ using $N = 50$. —, True density; Gaussian kernel estimate: ▲, $h = 0.20$; 0, $h = 0.45$; ---, polynomial kernel estimate with $h = 1.0$. For $x > 2.5$ the estimated density falls below the true density so that the total mass is identical for both densities.

both of which have continuous first derivatives. The mean error was estimated from (3.7) with $a = -1.5$, $b = 2.5$, and $m = 40$.

It can be seen from Fig. 1 that the Gaussian kernel gives a good estimate of the true density for a wide range of h. The kernel $P(u)$ give a much less satisfactory density estimate. Inspection of the particle positions when $P(u)$ is used shows that the particles tend to cluster an intervals of $\sim h$. If the number of particles is increased the number of particles in a cluster increases, the separation remains $\sim h$, and the accuracy is not improved. If h is made sufficiently small clustering ceases, but the accuracy is poor. We have found similar results with other kernels which are zero for $|u| \geqslant h$ and have continuous first derivatives which vanish at $u = 0$. Clearly, kernels like $P(u)$ should be avoided in hydrodynamical calculations.

In Fig. 2 we show the variation of the mean error with h for different values of N when the kernel $G(u)$ is used and the two different expressions for the term $[\nabla\rho/\rho^n]$ are used in (3.6). When $[\nabla\rho/\rho^n]$ is based on (2.18) the error has a minimum value at a value of h which decreases, as expected, with N. If h is $\gg$ optimum, the error $\propto h^2$ and is similar to the bias. When h is $\ll$ optimum, the error reflects the inability of the settling down process to produce a ρ_{SN} close to ρ_S. When $[\nabla\rho/\rho^n]$ is based on (2.23) the error is almost entirely due to bias and it can be made very small by reducing h.

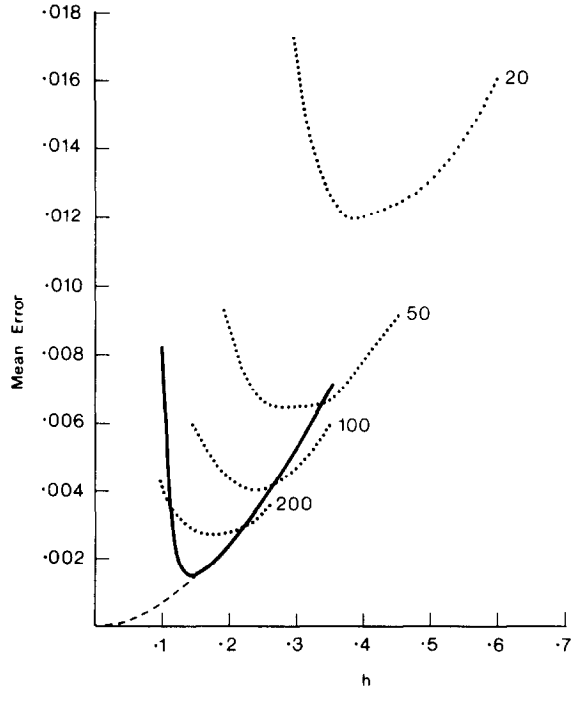

FIG. 2. Mean error as a function of h for different N. ···, With $\nabla\rho/\rho$ calculated from (2.18) the error with N the number alongside the curve; —, with $\nabla\rho/\rho$ calculated analogously to (2.23) the error with $N = 100$; ---, approximate theoretical estimate of the bias.

If h is sufficiently small the error eventually increases because the particles will then occupy only a very small part of the domain $(-1.5 \leqslant x \leqslant 2.5)$ in which the mean error is computed.

These results show that the Gaussian kernel can give density estimates with a mean error $\lesssim 1\%$ with only a small number of particles. Furthermore it suggests that the pressure estimate (2.23) is more accurate than the pressure estimate (2.18), though this result may depend on the equation of state.

4. Choosing the Smoothing Length

The usual practice in particle methods is to keep the grid and the length scale of any smoothing functions fixed during the course of a calculation. The smoothing length h of the effective kernel is therefore fixed and this must lead to loss of accuracy in problems involving collapse, expansion or disintegration.

For the problems we consider it is sometimes essential to alter h during the calculation. We achieve this by estimating h from the particle positions, choosing as an estimator a function which relates h to a natural length scale. We have used various functions for this purpose (Gingold and Monaghan [9, 10]). For problems involving self-gravitation the gravitational energy provides a natural length scale, and we have found that an h estimated from this length scale is convenient and accurate. Another convenient and more general estimate of h can be found by solving the equation

$$\sum_j \sum_k e^{-(\mathbf{r}_j - \mathbf{r}_k)^2/h^2} = \gamma = \text{const.} \tag{4.1}$$

The expected value of (4.1), in the limit of very small h, shows that

$$h \propto 1/\langle \rho \rangle^{1/d}, \tag{4.2}$$

where the average of ρ is a mass average and d is the number of dimensions. The use of (4.1) therefore results in an h which is weighted towards the mean particle separation in the high-density regions.

Since h depends on the particle positions the equations of motion (2.26) based on the Lagrangian (2.25) require derivatives of h to be included if energy is to be conserved very accurately. The resulting equations are complicated. We have found, however, that if these terms are omitted, energy is conserved with an error $< 1\%$ in isothermal collapse problems when the number of particles is $\gtrsim 400$ and the time step is chosen according to the procedure described in the Appendix. The conservation is improved as N is increased.

Intuitively it appears plausible that the accuracy will be increased if a separate h is chosen for each particle. We expect

$$h_j \propto 1/\rho_j^{1/d}. \tag{4.3}$$

For a Gaussian kernel this can be achieved by determining h_j from the rule

$$\sum_{i=1}^{N} e^{-(\mathbf{r}_i-\mathbf{r}_j)^2/h_j^2} = \sigma = \text{const.} \tag{4.4}$$

The left-hand side of (4.4) can be interpreted as roughly the number of neighbours in a sphere of radius h_j and the rule requires that this number be constant. Taking the expected value of (4.4) we find, for sufficiently small h, that (4.3) is obtained. The use of different h's means that

$$\rho_{SN}(\mathbf{r}) = \frac{M}{N} \sum_{j=1}^{N} (f_j/\pi)^{d/2}\, e^{-f_j(\mathbf{r}-\mathbf{r}_j)^2}, \tag{4.5}$$

where $f_j = 1/h_j^2$. The normalization is therefore retained and the mass is conserved.

In Fig. 3 we show the smoothed particle estimate (with both a single h and with an h for each particle) of the density

$$(4e^{-16x^2} + 3e^{-x^2})/4\sqrt{\pi}, \tag{4.6}$$

chosen because it has two, widely different, length scales. Various density estimates with a single h in the range $0.15 \leqslant h \leqslant 0.50$ were tried, and the results shown are typical. The maximum error in the variables h estimate is approximately $\frac{1}{6}$th the maximum error in the constant h estimate.

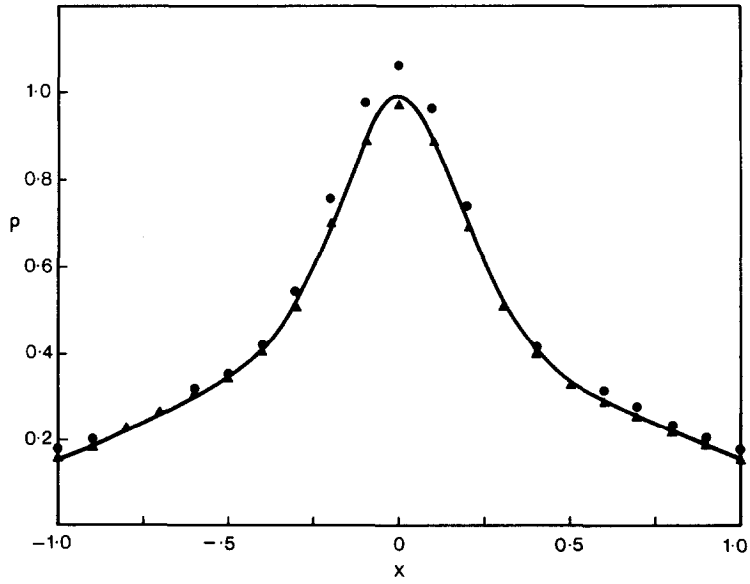

FIG. 3. Kernel estimate of the density defined by (4.6). ●, Gaussian kernel with the same $h = 0.2$ for each particle; ▲, Gaussian with a different h for each particle and σ in (4.4) = 6;—, density (4.6).

TABLE I

Error in the Gaussian Kernel Estimates of the Gambel Density Using a Different h for Each Particle[a]

σ	Range of f	Range of h	Mean error ($\times 10^{-3}$)	Max error ($\times 10^{-3}$)
4	$3.8 < f < 63$	$0.13 < h < 0.51$	2.3	5.3
6	$2 < f < 28$	$0.19 < h < 0.71$	1.3	3.6
8	$1.3 < f < 15$	$0.26 < h < 0.88$	2.2	4.5
10	$1 < f < 9.4$	$0.33 < h < 1$	1.1	2.7
15	$0.4 < f < 3.8$	$0.51 < h < 1.6$	1.1	1.9
20	$0.3 < f < 2.2$	$0.67 < h < 1.8$	3.2	5.3

[a] $N = 50$ and σ is defined by (4.4).

In Table I we show the errors in the variable h fit to the Gambel density when $N = 50$ and various σ (defined by (4.4)) are used. Although the minimum mean error is only comparable to that obtained with fixed h and illustrated in Fig. 2, it is much less sensitive to the choice of parameters and is therefore preferable in some numerical calculations. The improved resolution that can be obtained is a further advantage.

A disadvantage of assigning a separate h to each particle in a dynamical calculation is that the calculation time is longer, both because the equations are more complicated and because h must be updated for each particle at each time step. In addition, as explained in the Appendix, the gravitational force on a particle is the force on its smeared out density and this is not, in general, the force on a point particle at the center of the smeared out density. For the foregoing reasons we have only made a partial exploration of the use of an h for each particle (for an example see Section 7c).

5. Applications

SPH has been applied (Gingold and Monaghan [9]) to the problem of determining the static structure of both uniformly rotating and magnetic barytropic stars. These early calculations used an equation of motion which gave poor energy conservation, but the static structures were only in error by $\lesssim 2\%$ with $N = 80$.

Dynamical sequences for damped, rotating barytropic stars leading to fission have been examined (Gingold and Monaghan [10, 11] using Eqs. (2.26) with the addition of gravitational forces). The smoothing length h was the same for each particle and it was chosen by relating it to a length scale constructed from the gravitational energy. Since h is then a function of the particle coordinates, very accurate energy conservation requires that derivatives of h appear in the equation of motion. These were

small (< 1%) error in energy conservation in violent hydrodynamic processes (with an isothermal equation of state). The fission calculations showed that increasing the number of particles from 80 to 800, altering the initial particle positions, or changing the smoothing length by up to 50%, resulted in the global properties (energy, mean angular velocity, mean squared radius) changing by < 5%. The overall accuracy was further confirmed by the occurrence of changes of form in agreement with theory.

The calculations referred to do not establish that the details of hydrodynamic phenomena are described by SPH. We have therefore considered several further calculations, three of which are described below.

(a) *Isothermal Shocks*

The problem is that described in [4, Section IVa]; viz., the development of an isothermal one-dimensional shock from an initial state consisting of a high-density plateau surrounded by a region where the density is half as large. We represent the gas by 94 particles which were distributed regularly in $-48 < x < 171$, together with 10 fixed particles exterior to each low-density region. The region affected by the

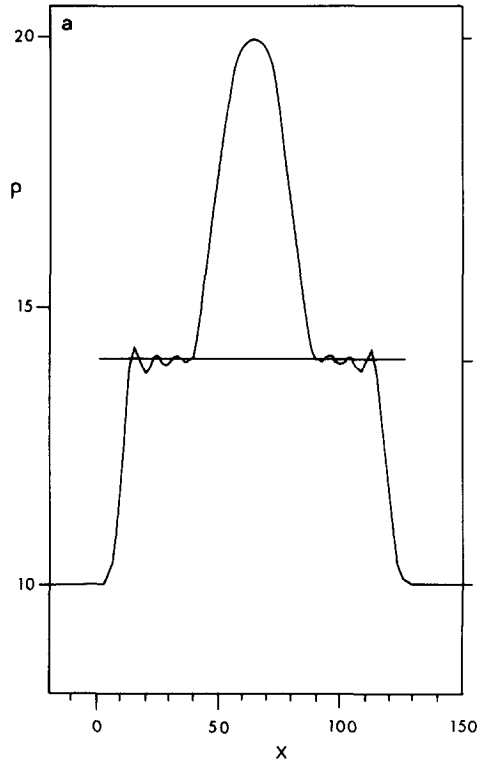

FIG. 4. (a) Density and (b) velocity profiles resulting from a isothermal-expansion shock in one-dimensional $N = 94$, $h = 3$ and the Gaussian kernel is used. The horizontal bars show the density and fluid velocity in the intermediate region taken from the exact solution (see of [4, Section IV(a)]).

shock during the calculation was $0 < x < 128$. Because there is no boundary, and the particles do not extend to infinity in both directions away from the high-density region, there are edge effects, but these do not propagate back to affect the region of interest during the course of the calculation. The scaling used results in unit sound speed.

Initially there were 0.33 particles per unit length in the low-density region. We took $h = 3$ and used the Gaussian smoothing kernel

$$W(u) = (1/h\sqrt{\pi}) \exp(-u^2/h^2),$$

so that the equations of motion (2.26) become

$$\frac{d^2x_k}{dt^2} = \frac{2c_s^2}{h\sqrt{\pi}} \sum_{j=1}^{N} \left(\frac{1}{\rho_j} + \frac{1}{\rho_k}\right)(x_k - x_j)\, e^{-(x_k - x_j)^2/h^2}, \qquad k = 1, 2, \ldots, N.$$

where c_s is the speed of sound. These equations conserve momentum and the invariant

$$\tfrac{1}{2}\sum (\dot{x}_j^2 + c_s^2 \ln p_j).$$

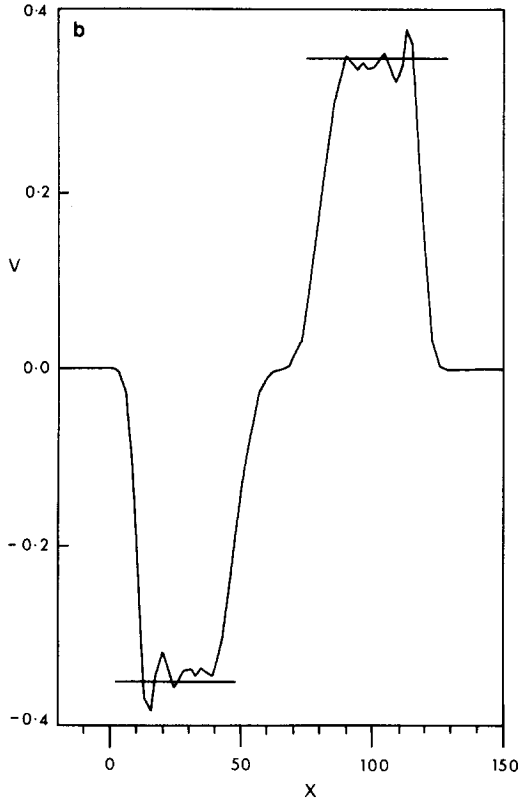

FIGURE 4 (continued)

The equations were integrated using the leapfrog scheme (Appendix). A small amount of generalized lax damping ($\alpha = 0.95$ in the Appendix) was introduced to reduce the postshock oscillations. Examination of the density and velocity profiles calculated both with and without damping, shows that with $\alpha = 0.95$ the oscillations are strongly damped without altering the transition width by more than a few percent.

Our results at $\tau = 20$ are presented in Fig. 4. The horizontal bars in the figure show the density of the intermediate region and its fluid velocity taken from the analytic solution given by LTD. The agreement is excellent. The shock velocity is measured to be $1.13c_s$, some 5% below the true value. This error is twice that quoted by LTD for their numerical calculations, but increasing the number of particles to 140 yields results to their accuracy. It should be noted that the particle method employed by LTD used 1920 particles while the SPH code used only 94 of which only 55 particles were actually in the region $0 < x < 128$. The shock front shown in Fig. 4, being smoothed over ~ 5 units, is much sharper than that found by LTD which was smoothed over ~ 10 units. The results are not sensitive to the choice of smoothing length. The value used above was chosen without prior experimentation.

(b) *Spherical Collapse of a Self-gravitating Pressureless Cloud*

In order to test the ability of SPH to estimate the density, to simulate the equation of continuity, and to provide accurate estimates of the gravitational forces, we have followed the collapse of a spherical cloud of pressureless particles. For any given initial mass distribution the exact solution can be computed easily.

The cloud considered has a mass of 1.989×10^{30} kg and an initial density distribution (not extending to infinity)

$$\rho = 4.39 \times 10^{-15} \exp(-\{r/4.6 \times 10^{14}\}^2) \quad \text{kg m}^{-3}.$$

The SPH calculation used $N = 2000$ with a Gaussian kernel. The initial value of h was 7×10^{13} m and it was varied during the calculation according to the rule used in [10]. In Fig. 5a we show the exact and SPH density fields after a time $t = 9.38 \times 10^{11}$ sec (equivalent to 0.93 free-fall times), when the central density has increased by a factor ~ 20. The accuracy of the SPH calculation is satisfactory except in the outermost layers where the spherical symmetry is not maintained accurately. This loss of accuracy is due to the small number of particles in this region.

In Fig. 5b we show the exact and SPH velocity fields at $t = 9.38 \times 10^{11}$ sec. Although the difference in the results is $\sim 10\%$ we regard it as satisfactory because small changes in time have a large effect on the fields when $t \sim$ free fall time. The SPH velocity field in Fig. 5b is similar to the exact velocity field at $t = 9 \times 10^{11}$ sec.

(c) *Spherical Collapse of an Isothermal Self-Gravitating Cloud*

We have used SPH to follow the isothermal collapse of an initially static cloud of one solar mass. The initial model is Penston's [12] case (ii) with a temperature of

5° K and molecular weight $\mu = 1$. For this case experiments with the pressure force calculated from (2.19) showed that satisfactory energy and momentum conservation could be achieved, and most of our calculations were performed using equations incorporating (2.19). Sequences were also run using an h for each particle. The calculations were carried out in three dimensions with no assumption of symmetry.

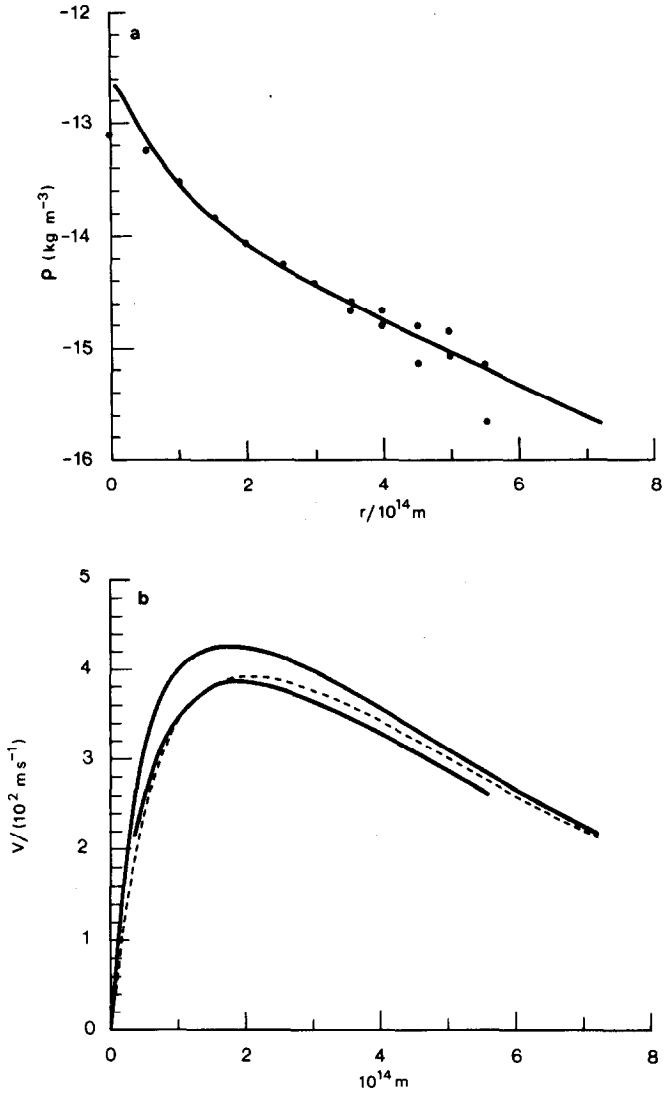

FIG. 5. (a) Density and (b) velocity profiles from the pressureless collapse of a self-gravitating cloud with mass 1.989×10^{30} kg and initial density given in Section 5b. $N = 2000$ and the initial $h = 7 \times 10^{13}$ m. The profiles are shown at $t = 9.38 \times 10^{11}$ sec (0.93 free fall times). (a) $h = 4.8 \times 10^{13}$ m; vertical scatter indicates degree of departure from spherical symmetry; (b) the upper curve is the exact velocity at $t = 9.38 \times 10^{11}$ sec, dashed curve $t = 9 \times 10^{11}$ sec, and lower curve is SPH result.

A difficulty with collapse problems of this kind is that the outer boundary is not modelled accurately and errors are produced by particles moving outward from the outer layer of particles. Offsetting this difficulty is the fact that the solution rapidly reaches the similarity state with $\rho \propto 1/r^2$. The principal effect of different (though still static and spherical) initial states is to alter the time at which a given density profile is reached (Bodenheimer and Sweigart [13]).

In Fig. 6 we show the density profiles calculated using SPH with $N = 400$ and $N = 2000$ after 1.5 free-fall times. They may be compared with the profiles calculated using a standard finite-difference Lagrangian code with 50 and with 300 shells also shown on Fig. 6. The agreement between the two SPH calculations and these is quite satisfactory except, as expected, within a smoothing length of the origin. The error in this high-density region is not due simply to the fact that the density is high, but rather that it increases very rapidly within $\lesssim h$ of the origin. With constant resolution such features are smoothed out. Any finite-difference or particle method with fixed resolution would eventually strike this difficulty for these collapses. In the very low density region SPH is not very accurate because there are very few particles there. We also show in Fig. 6 results for a sequence with an h for each particle. As we noted in Section 4, we believe the poor accuracy is due to the representation of the gravitational force in this case.

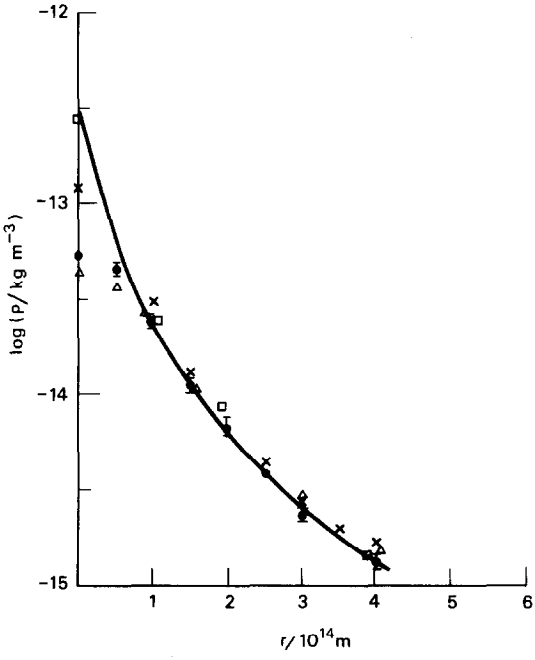

FIG. 6. The density profile of an isothermal self-gravitating cloud after 1.5 free-fall times. Mass, 2×10^{30} kg; temperature, 5° K; and molecular weight, 1. —, Finite difference with 300 shells; □, 50 shells; ×, SPH with $N = 2000$; △, SPH with $N = 400$; ●, with $N = 2000$ and h for each particle, with I to indicate the variation of ρ between axes.

The calculations made with a single h for the particles reveal an aspect of the kernel estimate method which is often overlooked. We refer to the fact that since the kernel estimate is based on a Monte Carlo estimate of an integral the error varies with N according to $1/\sqrt{N}$ regardless of the number of dimension. We therefore expect that the accuracy we achieve in a one-dimensional problem will be comparable to the accuracy achieved in a higher dimensional problem.

(d) *Tidal Interaction between Polytropic Stars and a Point Mass*

We present here a comparison between the SPH code and a linear normal mode analysis applied to the tidal interaction between a polytropic star of index 1.5 and a point of equal mass on a parabolic orbit. During periastron passage, energy is transferred from orbital motion to internal motion of the polytrope. This results in the polytrope becoming bound to the point mass on an orbit with semimajor axis a and eccentricity e. The extent of the interaction is a function of periastron separation δ_0. The fully three-dimensional SPH calculations employ 80 particles to represent an equilibrium polytrope approaching the point mass from infinity. The initial h was $\sim\frac{1}{4}$ of the radius of the unperturbed polytrope. It was altered during the calculation according to the rule given in [10]. The normal mode analysis examines the coupling with the orbital motion of the $l=2$ and $l=3$ linear nonradial pulsation modes of the polytrope.

Calculations were made for several orbits of different orbital angular momenta. The orbital elements (e and a) following the periastron passage are plotted as crosses (SPH calculation) in Fig. 7. The results of the normal mode analysis are shown by

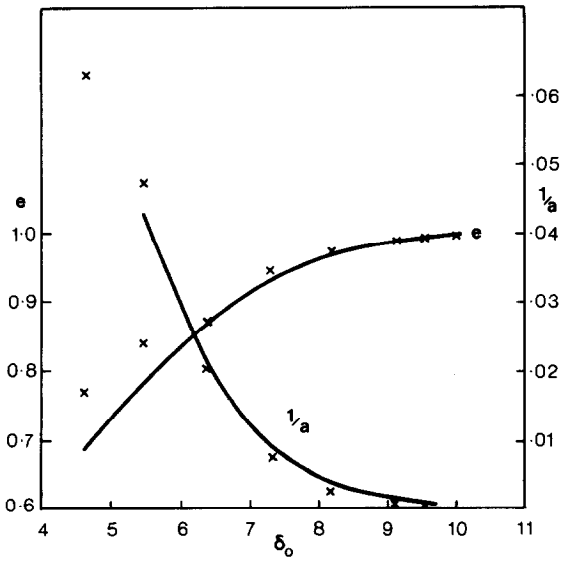

FIG. 7. The orbital parameters (eccentricity e, and semimajor axis a) resulting from the capture of a polytropic star by a point mass on a parabolic orbit with periastron separation δ_0. —, Normal mode analysis; ×, SPH results. Details are given in Section 5d.

the curves. Note that the energy transfer involved in achieving an orbit with $1/a = 0.02$ is $\sim 10\%$ of the polytrope's binding energy. Thus for $\delta_0 \lesssim 6$ (in units where the polytropic radius is 3.7) the linear analysis is inappropriate. The agreement in the linear regime can be seen from the figure to be quite good. The distortion and rotation of the polytrope is also similar in both calculations. A more detailed discussion can be found in [14].

6. Discussion and Conclusions

The traditional use of a grid in particle methods is apparently due to the belief that the only efficient way to compute spatial derivatives in hydrodynamics is to use finite differences. Finite-difference schemes based on the Lagrangian picture had the disadvantage that the grid had to be reformed in regions of high shear, while those based on the Eulerian picture had the disadvantage that the advection terms were difficult to represent by finite differences accurately. Harlow's combination of particles and grid was designed to retain the convenient fnite-difference mesh of the Eulerian picture while overcoming the advection problem by moving the particles of gluid in general agreement with the Lagrangian picture.

Our point of departure has been to recognize that spatial derivatives can be performed easily, without using finite derivatives, if kernel estimation is used. The Eulerian mesh is therefore superfluous. The analysis we have given of particle–grid methods shows that in their simplest form they are based on kernel estimation, but with a kernel that has two disadvantages. The first of these is that the kernel is unnecessarily complicated, and the second is that the resolution the kernel allows is not optimal because it is limited by the grid spacing. The direct kernel estimation method (SPH) makes use of a simple kernel and its resolution is determined by the particle separation which is necessarily less than any realistic grid spacing.

In common with other particle methods, SPH conserves linear and angular momentum exactly. We have not considered problems involving energy transport equations, but for the class of isentropic and isothermal equations of state used in this paper, the energy is conserved to better than 2%, and greater accuracy could be achieved with a smaller time step.

The experiments described in Section 5 indicate that with a relatively small number of particles (we have never used more than 2000) quite satisfactory accuracy can be obtained. A typical example is the isothermal shock problem where SPH, with 140 particles, gives an accuracy equivalent to LTD with 1920 particles. The spherical collapse of dust and isothermal gas clouds described in Section 5b and c shows that SPH models the dynamics and preserves the symmetry with acceptable accuracy despite the fact that the density increases by greater than one order of magnitude. The good agreement between the normal mode treatment of tidal interactions, and the SPH calculation described in Section 5d which uses only 80 particles, shows that SPH gives a good description of a non-spherical process in three dimensions.

A major contribution to the accuracy of SPH is due to the fact that its resolution

is better than the grid based methods. The resolution affects the accuracy through the bias in the kernel estimates. Both the SPH kernel used here, and the effective kernels in CIC, GAP, and LTD, have a first bias term which is quadratic in the smoothing length. The resolution is directly proportional to the smoothing length, and we therefore expect the SPH bias to be less.

We have discussed the relative merits of various kernels. Our experiments suggest that certain kernels should be avoided (see Section 3), but we expect kernels similar to the Gaussian (infinite domain, with the function symmetric, bounded, and with continuous first and second derivatives) to give very similar results. It is for this reason that we expect CIC, GAP, and LTD to give very similar results in hydrodynamic problems. An increase in accuracy may be achieved by using bias reducing kernels, an example of which is given in Section 4, but we have only partially explored their use in hydrodynamics. A further avenue for increased accuracy may lie in the use of a smoothing length for each particle. This device is of course analogous to a variable grid length in the Eulerian picture. Our experiments show that a very good fit to a specified density can be achieved using an h for each particle. The collapse calculation with an h for each particle, however, gave poor results.

Although we have discounted the use of a grid in estimating, it can be used as a convenient bookkeeping device to count those particles, usually within a range of $3h$, which give the dominant contribution to density, pressure, and thermal energy estimates. The grid also has advantages when other fields must be calculated. In the case of the gravitational field, which has a long range, the resolution required in computing $\nabla P/\rho$ is not needed. We would therefore recommend that the gravitational force be calculated from a grid when the number of particles is large.

APPENDIX

In this Appendix, unless the contrary is stated, we assume each particle has the same h.

(a) *Equations of Motion*

We construct the equation of motion using (2.23) for the pressure term. For the problems we consider, the body force is due to self-gravitation, and the gravitational force on a particle can be computed from the total gravitational energy. For inviscid, isentropic motion the resulting equations can be derived from the Lagrangian

$$L = \frac{M}{N} \sum_{j=1}^{N} (\tfrac{1}{2}\dot{\mathbf{r}}_j^2 - U(\rho_j) + \Omega_j), \tag{A1}$$

where U is the internal energy per unit mass, and

$$-\frac{M}{N} \sum_j \Omega_j \tag{A2}$$

is the gravitational energy. The density ρ_j at the position of particle j is given by the kernel estimate (2.5). The equations of motion of the kth particle takes the form

$$\ddot{\mathbf{r}}_k = -\sum_{j=1}^{N} [U'(\rho_j) + U'(\rho_k)] \left[\frac{\partial}{\partial \mathbf{r}_k} W(\mathbf{r}_k - \mathbf{r}_j; h)\right]_h + \frac{\partial}{\partial \mathbf{r}_k} \sum_j \Omega_j + \left[\frac{\partial}{\partial h} \sum_j (-U(\rho_j) + \Omega_j)\right] \frac{\partial h}{\partial \mathbf{r}_k}. \tag{A3}$$

For a general equation of state, $U' \equiv dU/d\rho$ should be replaced by P/ρ^2. In the following we assume N is sufficiently large to allow the contribution to (A3) from the ∇h term to be neglected.

(b) *Choosing and Updating h*

If h is determined from, for example, the equation

$$\sum_i \sum_j e^{-(\mathbf{r}_i - \mathbf{r}_j)^2/h^2} = \gamma, \tag{A4}$$

then γ is fixed by requiring h to give a density in good agreement with the specified initial density specified. For the tidal interaction problem (Section 5c) a damping term $\propto \dot{\mathbf{r}}_k$ was initially added to (A3) to produce a settled-down polytrope which was then placed in orbit about the point mass. For the isothermal collapse (Section 5b) the initial positions of the particles and the initial h were fixed by using equations analogous to (3.7).

For a given γ, h can be calculated from (A4) using the Newton–Raphson rule. A quicker method is to update h using

$$\frac{dh}{dt} = \sum_k \frac{\partial h}{\partial \mathbf{r}_k} \cdot \dot{\mathbf{r}}_k. \tag{A5}$$

(c) *The Gravitational Energy*

Equation (A2) is an estimate of

$$-\frac{G}{2} \iint \frac{\rho(\mathbf{r})\,\rho(\mathbf{r}')}{|\mathbf{r} - \mathbf{r}'|}\, d\mathbf{r}\, d\mathbf{r}'. \tag{A6}$$

This integral can be evaluated with sufficient accuracy by one Monte Carlo integration followed by an exact integration using a kernel estimate of the density. We find (A6) becomes

$$-\frac{G}{2} \left(\frac{M}{N}\right)^2 \sum_j \sum_a \int \frac{W(\mathbf{r}' - \mathbf{r}_a, h)}{|\mathbf{r}' - \mathbf{r}_j|}\, d\mathbf{r}'. \tag{A7}$$

If we use a Gaussian kernel in three dimensions, (A3) becomes (with $f = 1/h^2$ and $\mathbf{u}_{kj} = \mathbf{r}_k - \mathbf{r}_j$)

$$\ddot{\mathbf{r}}_k = 2f\left(\frac{f}{\pi}\right)^{3/2} \sum_{j=1}^{N} \left[\frac{p_j}{\rho_j^2} + \frac{p_k}{\rho_k^2}\right](\mathbf{r}_k - \mathbf{r}_j)\, e^{-fu_{kj}^2} + \frac{GM}{N}\frac{2}{\sqrt{\pi}} \sum_{j=1}^{N} \left\{-\frac{1}{u_{kj}^2}\int_0^{u_{kj}\sqrt{f}} e^{-y^2}\, dy + e^{-fu_{kj}^2}\right\} \frac{(\mathbf{r}_k - \mathbf{r}_j)}{u_{kj}}. \tag{A8}$$

The error function, and the exponentials in (A8), can be calculated economically by interpolation.

Note that the gravitational force on particle k is the force on the smoothed out density centred on particle k, and that the force on k due to j is equal and opposite to the force on j due to k as expected.

(d) *Time Integration*

To integrate (A7) we use the simple leapfrog scheme

$$\mathbf{v}_k^{n+1/2} = \mathbf{v}_k^{n-1/2} + \overline{\delta t}\, \mathbf{F}_k$$

and

$$\mathbf{r}_k^{n+1} = \mathbf{r}_k^n + \delta t^{n+1}\, \mathbf{v}_k^{n+1/2}, \tag{A9}$$

where $\overline{\delta t} = 0.5\ (\delta t^n + \delta t^{n+1})$ and $\mathbf{F}_k$ is the right-hand side of (A7). If damping of shock oscillations is required, we generalize Lax's method by replacing the first of (A8) by

$$\mathbf{v}_k^{n+1/2} = \alpha \mathbf{v}_k^{n-1/2} + (1-\alpha)\, \mathbf{v}_{ks} + \overline{\delta t}\, \mathbf{F}_k, \tag{A10}$$

where $\mathbf{v}_{ks}$ is the smoothed velocity

$$\mathbf{v}_{ks} = \frac{M}{N} \sum^{N} \frac{\mathbf{v}_j^{n-1/2}}{\rho} W(\mathbf{r}_k - \mathbf{r}_j). \tag{A11}$$

In Lax's scheme the velocity is averaged over adjacent grid points. Equation (A10) has a similar effect since $\mathbf{v}_{ks}$ is a velocity which is weighted average over particles in the neighbourhood of particle k.

The time step was chosen by finding

$$s = \min\left(\frac{h}{|\mathbf{v}_j|}, \left(\frac{h}{|\mathbf{F}_j|}\right)^{1/2}, \frac{h}{c_{sj}}\right), \qquad j = 1, 2, \ldots, N \tag{A12}$$

where c_{sj} is the speed of sound at the jth particle, then taking

$$\delta t = \lambda s.$$

For the calculations reported here $\lambda < 0.5$ is sufficient.

(e) *Separate h for Each Particle*

If we have a separate h for each particle the symmetry of the forces is only maintained if, in (A6), we replace both densities by their kernel estimates. We find (A6) becomes

$$-\frac{G}{2}\left(\frac{M}{N}\right)^2 \sum_j \sum_a \frac{1}{u_{aj}} \frac{2}{\sqrt{\pi}} \int_0^{gu_{aj}} e^{-y^2}\, dy, \tag{A13}$$

where

$$g = [f_a f_j/(f_a + f_j)]^{1/2}, \tag{A14}$$

and $f_j = 1/h_j^2$. Again neglecting $\partial h_j/\partial \mathbf{r}_k$ terms, the gravitational force on particle k is

$$G\frac{M}{N}\frac{2}{\sqrt{\pi}} \sum_{j=1}^{N} \left\{ -\frac{1}{u_{kj}^2} \int_0^{u_{kj}g} e^{-y^2}\, dy + e^{-gu_{kj}^2} \right\} \frac{(\mathbf{r}_k - \mathbf{r}_j)}{u_{kj}}. \tag{A15}$$

If particle k is at the point with the lowest density it has the largest h and smallest f. Accordingly, $g \sim \sqrt{f_k}$, and the gravitational force is equivalent to considering all other particles smoothed with the length scale h_k. Thus the requirement that the symmetry be maintained demands also that the force on the particle at $\mathbf{r}_k$ be the force on the smeared-out density which is centred at $\mathbf{r}_k$ and has the same mass as the particle. This is not the force on a point particle at r_k since this would be the same as the gravitational force in (A7) with each f replaced by f_j.

The equations of motion for this case become

$$\ddot{\mathbf{r}}_k = \frac{2}{\pi^{3/2}} \sum_{j=1}^{N} (\mathbf{r}_k - \mathbf{r}_j)[f_k^{5/2} U'(\rho_j) \exp(-f_j u_{kj}^2) + f_j^{5/2} U'(\rho_k) \exp(-f_j u_{kj}^2)] + \text{gravitational force}, \tag{A16}$$

where the gravitational force is given by expression (A15).

Acknowledgments

This work was completed with the support of ARGC Grant B7715346R. Our work was stimulated by the lectures of L. Lucy at the Institute of Astronomy, Cambridge, in 1976, in which he suggested, and gave examples of, the use of statistical estimation in hydrodynamics.

References

1. J. Von Neumann, "Collected Works" (A. H. Taub, Ed.), Vol. 6, p. 361, Pergamon, Oxford, 1963.
2. J. R. Pasta and S. Ulan, *Math. Tables Other Aids to Comput.* **13** (1959), 1.
3. R. Larson, *J. Comput. Phys.* **27** (1978), 397.

4. J. N. LEBOEUF, T. TAJIMA, AND J. M. DAWSON, *J. Comput. Phys.* **31** (1979), 319.
5. M. ROSENBLATT, *Ann. Math. Statist.* **27** (1956), 832.
6. M. ROSENBLATT, *Ann. Math. Statist.* **42** (1971), 1815.
7. L. I. BONEVA, D. KENDALL, AND I. STEPANOV, *J. Roy. Statist. Soc.* **33**, (1971), 1.
8. C. ECKART, *Phys. Fluids.* **3** (1960), 421.
9. R. A. GINGOLD AND J. J. MONAGHAN, *Mon. Not. Roy. Astron. Soc.* **181**, (1977), 375.
10. R. A. GINGOLD AND J. J. MONAGHAN, *Mon. Not. Roy. Astron. Soc.* **184**, (1978), 481.
11. R. A. GINGOLD AND J. J. MONAGHAN, *Mon. Not. Roy. Astron. Soc.* **188**, (1979), 39.
12. M. V. PENSTON, *Roy. Obs. Bull.* No. 117 (1966).
13. P. BODENHEIMER AND A. SWEIGART, *Astrophys. J.* **152** (1968), 515.
14. R. A. GINGOLD AND J. J. MONAGHAN, *Mon. Not. Roy. Astron. Soc.* **191** (1980), 897.